Chemical Papers (2024) 78:4495–4506
https://doi.org/10.1007/s11696-024-03413-6

ORIGINAL PAPER

Determination of lead and cadmium by magnetic solid-phase extraction (MSPE) using Co_3O_4@Fe_3O_4 nanoflowers and flame atomic absorption spectrometry (FAAS)

Şeyma Korkmaz[1] · Nurdan Kurnaz Yetim[1] · Mümin Mehmet Koç[2,3] · Cemile Özcan[1]

Received: 8 July 2023 / Accepted: 9 March 2024 / Published online: 5 April 2024

Abstract

Heavy metal ions penetrate wastewater and clean water sources, leading to environmental pollution which adversely affecting human health. The determination and extraction of metal ions help to prevent unwanted effects on the environment and human health. Solid phase extraction method is used for the removal of heavy metal ions. Such method is rapid, reliable and affordable method which provide high recovery rate. For this purpose, cobalt(II/III) oxide@iron(II/III) oxide (Co_3O_4@Fe_3O_4) core–shell composite nanoflowers were fabricated via hydrothermal synthesis for the recovery of heavy metal ions (Pb^{2+} and Cd^{2+}). X-ray diffraction (XRD), scanning electron microscopy (SEM), energy dispersive X-ray spectroscopy (EDX), and vibrating sample magnetometry (VSM) were used in the chemical and structural characterization of Co_3O_4@Fe_3O_4. Flame atomic absorption spectrometry (FAAS) was used for the determination of total metal content. In our work, optimum conditions for heavy metal on recovery such as eluent concentration, eluent type, pH, adsorbent amount, solution volume, sonication duration, were studied. As a result of these studies, quantitative recovery of analyte ions was obtained at pH 7.5. Quantitative recovery of Pb^{2+} ions was observed with 20 mL 1 M HNO_3 solution as eluent and 100 mg amount of adsorbent while, they were found for Cd^{2+} ion recovery with 5 mL 1 M HNO_3 solution as eluent and 200 mg amount of adsorbent. The highest recovery rates were found to be 99.6% and 99.9% for Pb^{2+} and Cd^{2+} heavy metal ions, respectively.

Keywords Magnetic solid-phase extraction (MSPE) · Co_3O_4@Fe_3O_4-doped nanoflowers · Flame atomic absorption spectrometry (FAAS)

Introduction

Water is essential for each organism on the planet. It is a known fact that there is a limited source of water. Industrial activities require a vast amount of water, where the water used in the course of pursuing such activities usually ends up contaminated. Heavy metal ions are among the most dangerous contaminants which can be found in such waters (Khan et al. 2019; Morrow 2010). Lead, zinc, chromium, copper, mercury, arsenic, and cadmium are commonly found in wastewater (Alp Kavlo et al. 2023; Dağci et al. 2021; Goudarzi 2007; Kaya et al. 2010; Khan et al. 2022; Kurnaz Yetim et al. 2022). Heavy metal ions can be released through natural processes and human activities such as various industrial activities, mining, agriculture. (Jagirani et al. 2021; Kaya et al. 2010; Ozcan et al. 2018). Once heavy metal ions are released, they can have both short- and long-term impacts on soil and water ecosystems which can have a range of both direct and indirect consequences is better (Elliott et al. 1986; Ozcan et al. 2018; Raskin et al. 1994; Saleh et al. 2022).

Heavy metal ions can be bioaccumulated in tissues, which can have a deleterious effect on the food chain (Özdemir et al. 2019). Similarly, the release of heavy metal-containing waters can also contaminate the soil, where heavy metal ions can build up in vegetation (Cheng 2003; Elliott et al. 1986; Ozcan et al. 2018; Rascio et al. 2011; Raskin et al. 1994; Saleh et al. 2022). Heavy metal ions can damage the genetic

✉ Cemile Özcan
cemilebal.ozcan@klu.edu.tr

[1] Department of Chemistry, Faculty of Arts and Sciences, Kırklareli University, Kırklareli, Türkiye

[2] Department of Physics, Faculty of Arts and Sciences, Kırklareli University, Kırklareli, Türkiye

[3] School of Medical Service, Kırklareli University, Kırklareli, Türkiye

materials of such organisms, disrupt their metabolic processes, and can lead to immune-related dysfunctions (Guo et al. 2009; Sultana et al. 2019; Zhou et al. 2008). Moreover, consumption of heavy metal exposed foods can lead to indirect intake of heavy metals (Khan et al. 2022; Sultana et al. 2019), which can have long-term effects on humans (Gacía et al. 2018; Gupta et al. 2015; Ijomone et al. 2020; Lin et al. 2018; Mishra 2009; Zheng et al. 2023, 2012).

Prevention and mitigation of heavy metal ions from entering freshwater are essential to minimizing any potential direct effects. Traditional wastewater management technologies may have certain limitations in terms of removing heavy metal ions. To this end, innovative technologies are required to deal with any such issues. At this point, one such technology that has great potential is nanoparticles, which may be used in the removal of heavy metal ions (Salem et al. 2017; Xiong et al. 2015).

Nanoparticles are very small particles the diameter of which is between a couple of nanometres to a few hundred nanometres (Yu et al. 2006). They exhibit interesting chemical, physical, and electronic properties compared to the bulk material. Nanoparticles have large surface area/volume ratios, as noted by Xu et al. (2012), which makes them suitable candidates for heavy metal absorption. A high surface area/volume ratio also leads to high electron concentration on the surface, which also leads to high reactivity (Xu et al. 2012). Hence, high catalytic activity can be obtained from such. Various types of nanostructures have previously been reported regarding their applications in heavy metal recovery. Among those, metallic nanoparticles are of some particular importance due to their unique properties. The heavy metal removal characteristics of Bi nanoparticles, Ti nanoparticles, Au nanoparticles, Mg nanoparticles, and Ag nanoparticles have previously been reported (Guevara-bernal et al. 2022; Kurnaz Yetim et al. 2022; Lo et al. 2012; Mahdavi et al. 2012; Qian et al. 2013; Razzaz et al. 2016; Talukder et al. 2022). In heavy metal removal applications, microextraction, liquid–liquid extraction, cloud point extraction, solid-phase extraction, dispersive liquid–liquid microextraction, and chemical precipitation methods have commonly been used (Alp Kavlo et al. 2023; Altunay et al. 2022; Goudarzi 2009; Habila et al. 2017; Kinaree et al. 2014; Kurnaz Yetim et al. 2022; Rihana-Abdallah et al. 2022; Saleh et al. 2022; Soylak et al. 2007; Taghani et al. 2018). In addition, the potential for heavy metal removal via magnetic nanoparticles has also been evidenced in the literature (Almomani et al. 2020; Dave et al. 2014). Depending on their magnetic properties, magnetic nanoparticles can display superparamagnetic, ferromagnetic, and ferrimagnetic properties. Iron oxide, cobalt oxide, and nickel oxide nanoparticles, for instance, are commonly used in magnetic nanoparticle applications (Karaçam et al. 2020; Kurnaz Yetim et al. 2020a; Yetim 2021). Producing composite nanostructures using such magnetic cores has been favoured in terms of obtaining nanocomposites with magnetic characteristics. Using magnetic nanoparticles in heavy metal ion removal provides certain advantages. For example, magnetic nanoparticles have quite a high potential for heavy metal removal (Wang et al. 2015; Zarei et al. 2018). In addition, magnetic nanoparticles can be collected by a simple magnet, which makes them suitable candidates for magnetic filtration applications (Kurnaz Yetim et al. 2020a).

The heavy metal adsorption characteristics of magnetic nanocomposites have been previously assessed in the literature. For example, Safinejad et al. assessed the removal properties of magnetic zeolites for Pb and Cd (Safinejad et al. 2017). Shishehbore investigated the heavy metal removal properties of silica-coated ferrite nanoparticles (Shishehbore et al. 2011). Warner et al. assessed the heavy metal adsorption potential of manganese-doped iron oxide nanoparticles (Warner et al. 2012). $Fe_3O_4@SiO_2$ nanocomposites were assessed for Ni, Cu, and Fe removal by Huang et al. (Huang et al. 2014). It may be noted, however, that the heavy metal removal properties of $Co_3O_4@Fe_3O_4$ nanoflowers have not previously been addressed in the literature.

In this report, $Co_3O_4@Fe_3O_4$ nanoflowers were produced via hydrothermal synthesis (Hasanoğlu Özkan et al. 2022). Cd^{2+} and Pb^{2+} heavy metal ion removal by $Co_3O_4@Fe_3O_4$ nanoflowers from seawater, mineral water, tap water, and bottled water was studied, and a new extraction enrichment method was developed. It can be seen in the literature that nanoflowers have been used in the removal of heavy metal ions (Aybike et al. 2023; Kurnaz Yetim et al. 2022; Ozalp et al. 2023); however, the report assess the potential of $Co_3O_4@Fe_3O_4$ composite nanoflowers for heavy metal removal.

Materials and methods

Spectral data measurements

A Rikagu Miniflex600 X-ray diffractometer that had a Ni-filtered Cu Kα source was used for the X-ray diffraction (XRD) analysis. The scanning range was $10° < 2\theta < 90°$ and signals obtained in the investigations were recorded. The peaks were identified using the software of the device and compared with the similar results in the literature. Additionally, scanning electron microscopy (SEM) was used to analyse the surface morphology of the nanoflowers. Analysis was performed in different electron energies 10 kV, 20 kV and 30 kV in back scattering mode and secondary electron mode. Images with acceptable visual quality were used in the assessment. The energy dispersive X-ray spectroscopy (EDX) analysis was performed during SEM investigation no additional investigation was

performed. For EDX analysis, a Fei Quanta 400F equipped with apparatus was used. Magnetic measurements were performed at room temperature by a vibrating sample magnetometer, Cryogenic Limited PPMS with the maximum magnetic field of ± 1 T. An Isolab ultrasound wave-supported ultrasonic bath was used in liquid extraction. A Quantachrome Corporation Autosorb-6 was used for the pore size characterization. After the recovery of analytes with MNP, measurements were made in the decanted and eluted solutions. An Agilent 240 AA Duo model atomic absorption spectrometer was used to perform the analytical work where the analytes. Pb and Cd, were identified using hollow cathode lamps (Agilent). The parameters for metal analysis can be shown in Table 1. The experimental process conducted in the work is shown in Fig. 1.

Table 1 Parameters pertaining to FAAS for metals

	Pb	Cd
Wavelength (nm)	283.3	326.1
Used flame	Air/acetylene	Air/acetylene
Acetylene flow (mL/min)	2.00	2.00
Slit width (nm)	0.5	0.5
Air flow (mL/min)	13.5	13.5
Lamp current (mA)	10.0	4.0

Merck quality chemicals and regents were used, which are of analytical grade. Ultrapure water with an 18.2 MΩ cm specific resistance was used in the experiments.

For standard solutions of metals, 1000 mg/L NIST standard stock solutions were used. The Pb and Cd standards to be analysed were prepared for the appropriate working range of 0.05–3 mg/L. Standard solutions were prepared by dissolving with 0.5 M HNO_3. Solutions of 0.05, 0.1, 0.25, 0.5, 1, 2, and 3 mg/L prepared from standards of Pb and Cd were read in the FAAS.

Synthesis of Co_3O_4@Fe_3O_4 nanoflowers

For the synthesis of Co_3O_4@Fe_3O_4 magnetic nanoflowers, Co_3O_4 was first synthesised via the hydrothermal method. For this purpose, 9.7 g of cobalt(II) nitrate hexahydrate ($Co(NO_3)_2.6H_2O$) and 0.5 g urea were stirred together using a magnetic stirrer for 1 h and dissolved in 35 mL deionized water. Then, the mixed solution was transferred into a 50 mL Teflon-lined autoclave. The mixture was kept there for 12 h at 160 °C. The suspension was cooled to room temperature and centrifuged. The sediment obtained from the suspension was washed several times with deionized water and ethanol. The resultant product was calcinated at ash oven at 300 °C and kept there for 1 h (Kurnaz Yetim et al. 2020b). The hydrothermal nanofabrication method was used to produce Co_3O_4@Fe_3O_4 nanoflowers. 0.656 g iron (II) sulphate

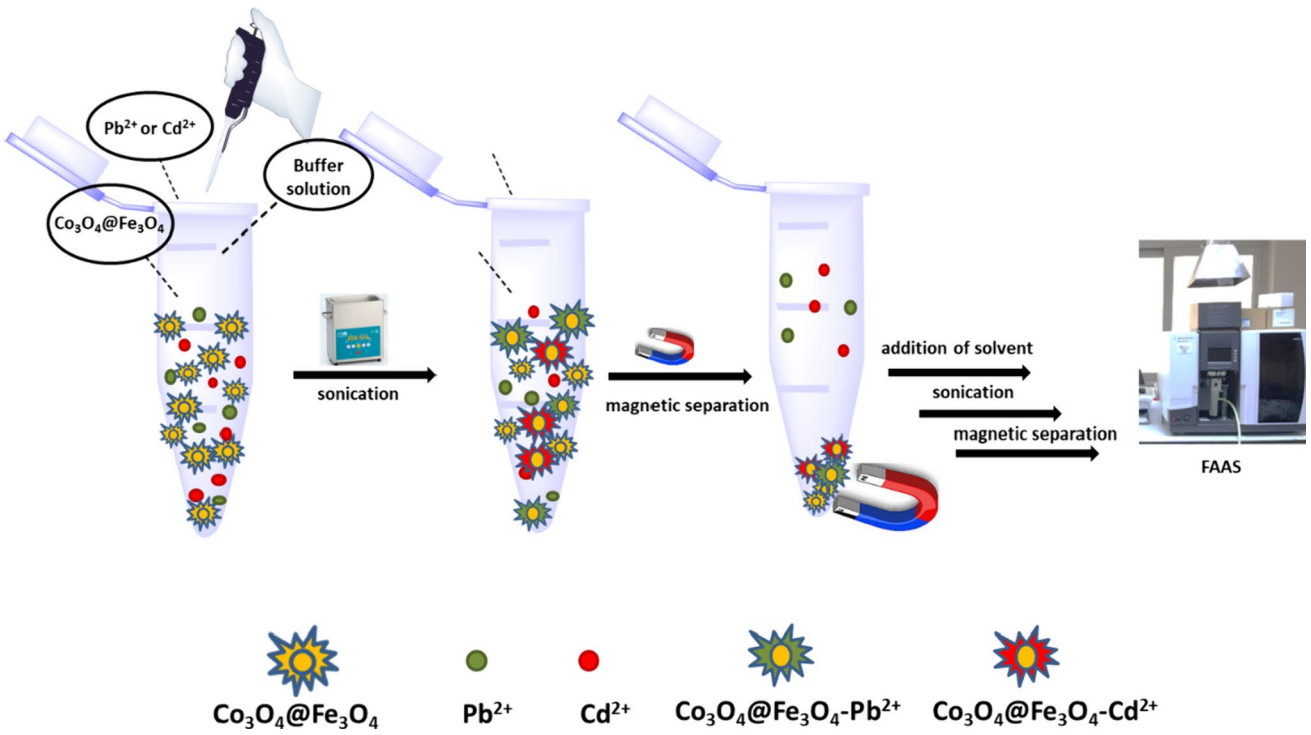

Fig. 1 Schematic summarizing the experimental workflow of the study

heptahydrate ($FeSO_4.7H_2O$) and 3.2 g NaOH were dissolved in 40 mL pure water and stirred for 15 min. In a second, separate beaker, 0.4 g Co_3O_4 was dissolved in 25 mL pure water and stirred for 10 min. Co_3O_4 mixture was added dropwise to the first mixture and stirred for 5 min. The final product was transferred to an autoclave and kept there at 150 °C for 6 h. The autoclave was then cooled at room temperature and the adsorbent was magnetically separated in solution using a magnet. The solid-phase was washed repeatedly with water and ethanol and then dried in an oven at 80 °C for 24 h (Hasanoğlu Özkan et al. 2022).

Solid-phase extraction procedure

The solid-phase extraction method used in the recovery of metal ions and the preparation of freshwater samples, seawater and standard reference materials (SRM) in Supplementary were shown. The same protocol is also shown in the Fig. 1.

Results and discussion

Characterization of Co_3O_4@Fe_3O_4 composite nanoflowers

XRD characterization of composite nanoflowers

X-ray diffraction patterns of Co_3O_4@Fe_3O_4 composite nanoflowers and Fe_3O_4 magnetic nanoparticles are shown in Fig. 2. It can be seen that the patterns are coherent with each other, where peaks related to Fe_3O_4 nanoparticles can be identified in the pattern of Co_3O_4@Fe_3O_4 composites. It can be seen that the sharpness of the peaks decreases subsequent to doping with Co_3O_4. However, the intensities of the peaks appear similar. No contamination-related peaks are shown in the pattern, indicating that the nanoparticles are of high purity.

The diffraction peaks related to Fe_3O_4 are shown with the orange lines in Fig. 2, where peaks at 18.3°, 30.4°, 35.6°, 37.08°, 43.3°, 53.36°, 57.3°, 62.8°, 70.98°, 74.12°, 74.98°, and 78.94° are defined, which correspond to the (1 1 1), (2 2 0), (3 1 1), (2 2 2), (4 0 0), (4 2 2), (5 1 1), (4 4 0), (6 2 0), (5 3 3), (6 2 2), and (4 4 4) face-centred cubic (fcc) crystal formations, respectively (Karaçam, Yetim, and Koç 2020; Kurnaz Yetim et al. 2020a). Co_3O_4 nanoflowers show two distinctive peaks at 36.8° and 38.5°, which illustrate fcc crystal structures with (3 1 1) and (2 2 2) orientations. The XRD pattern of Co_3O_4 nanoflowers exhibit peaks at 19.0°, 31.3°, 36.8°, 38.5°, 44.8°, 55.6°, 59.4°, 65.2°, and 77.3°, which are indicative of the (1 1 1), (2 2 0), (3 1 1), (2 2 2), (4 0 0), (4 2 2), (5 1 1) and (4 4 0) fcc orientations, respectively (Kurnaz Yetim et al. 2020b). The XRD pattern

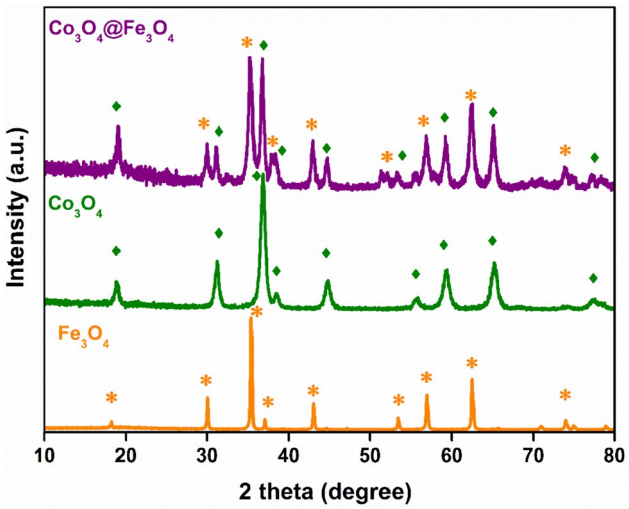

Fig. 2 X-ray diffraction patterns of Co_3O_4@Fe_3O_4 nanocomposites, and Co_3O_4 and Fe_3O_4 magnetic nanoparticles

of Co_3O_4@Fe_3O_4 nanoflowers is shown via a purple line in Fig. 2, which can be seen to contain peaks associated with Fe_3O_4 and Co_3O_4 (Hasanoğlu Özkan et al. 2022; Yetim 2021). The sharp and intense peaks seen in the XRD patterns indicate good crystallinity.

SEM and EDX analysis of Co_3O_4@Fe_3O_4 composite nanoflowers

The co-deposition of Co_3O_4 with Fe_3O_4 nanoparticles slightly alters the structure of the Co_3O_4. It can be seen that Fe_3O_4 nanoparticles fill the pores and gaps in the Co_3O_4 nanoflowers. The size of the Fe_3O_4 nanoparticles was found to be smaller than 100 nm; and therefore can easily fill the pores between spikes of Co_3O_4 nanoflowers. Figure 3 illustrates the SEM image, EDX spectra, and EDX mapping results for Co_3O_4@Fe_3O_4 nanoflowers. The SEM image confirms the clumpy structure of the Co_3O_4@Fe_3O_4 nanoflowers when the Fe_3O_4 nanoparticles fill the gaps in the former. The EDX spectrum contains Co-, O- and Fe-related peaks, which also confirms the chemical form of the Co_3O_4@Fe_3O_4 nanoflowers. The EDX maps also confirm that Co_3O_4@Fe_3O_4 nanoflowers consist of Co, Fe and O. It can be seen that Co accumulated on the inner sections of the nanoflowers, whereas Fe was found on the outer shell. O, by contrast, spreads all over the nanocomposites.

VSM analysis of magnetic composites

Vibrating sample magnetometry (VSM) results for Co_3O_4@Fe_3O_4 nanoflowers were assessed and the associated hysteresis plot is shown in Fig. 4. These hysteresis plots illustrate a large coercivity; therefore, it was deduced that Co_3O_4@

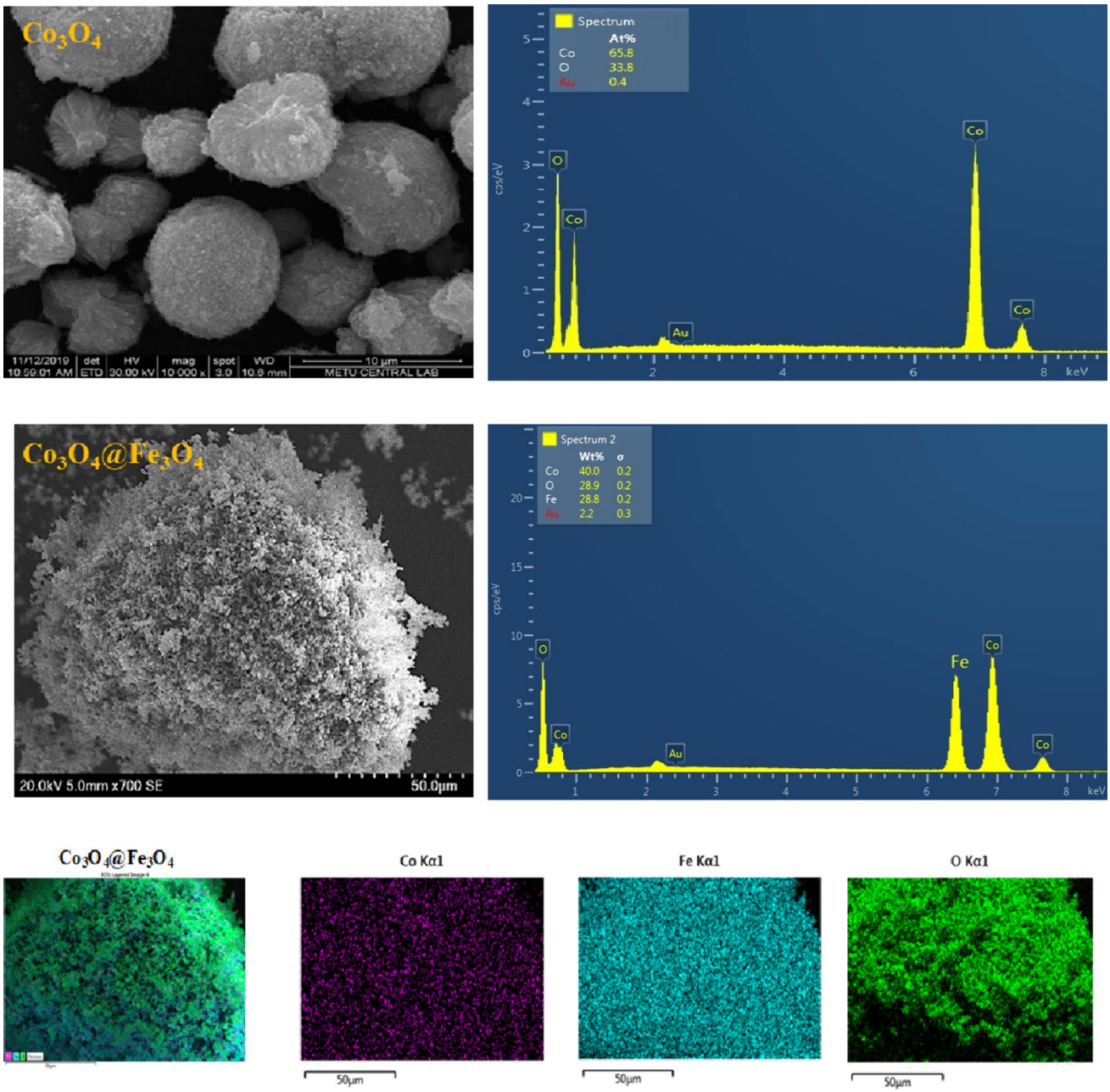

Fig. 3 Scanning electron microscopy image, energy dispersive X-ray spectra, and energy dispersive X-ray spectra mapping results for Co_3O_4@Fe_3O_4 nanoflowers (Hasanoğlu Özkan et al. 2022)

Fe_3O_4 nanoflowers exhibit ferromagnetic characteristics. The magnetic saturation of Fe_3O_4 was found to be around 90 emu/gr, while Co_3O_4@Fe_3O_4 nanoflowers were defined as being around 38.3 emu/g. It can be seen that the addition of Co_3O_4 to the Fe_3O_4 structure slightly decreases the overall magnetic saturation. In all, the magnetic saturation of Co_3O_4@Fe_3O_4 nanoflowers was found to be quite high compared to the nanoflower-based magnetic composites. Different magnetic saturations have been reported in the literature for Fe_3O_4 nanostructures; for instance, the magnetic saturation of Bi_2S_3@Fe_3O_4 was found to be between 2.24 emu/g and 28.6 emu/g (Karaçam et al. 2020), and as 22.1 emu/g for Fe_3O_4@SiO_2 magnetic nanoparticles (Tumturk et al. 2014). The magnetic saturation of Fe_3O_4@G2 and Fe_3O_4@G2/Au/Bi magnetic nanocomposites were found to be 34.7 emu/g and 34.4 emu/g, respectively; that of Fe_3O_4–PbS nanostructures was found to be 8.2 emu/g (Hedayati et al. 2016), and those of Fe_3O_4/gelatine/metoprolol and Fe_3O_4/gelatine/aspirin were determined to be 3.5 emu/g and 8 emu/g, respectively (Kavousi et al. 2019).

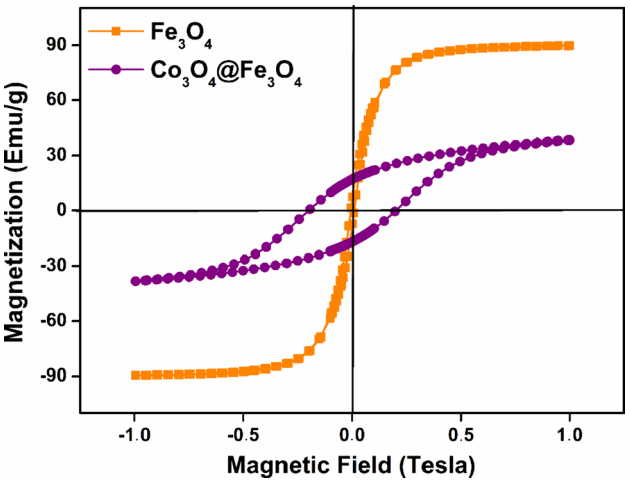

Fig. 4 Vibrating sample magnetometry characteristics of Co_3O_4@Fe_3O_4 nanoflowers

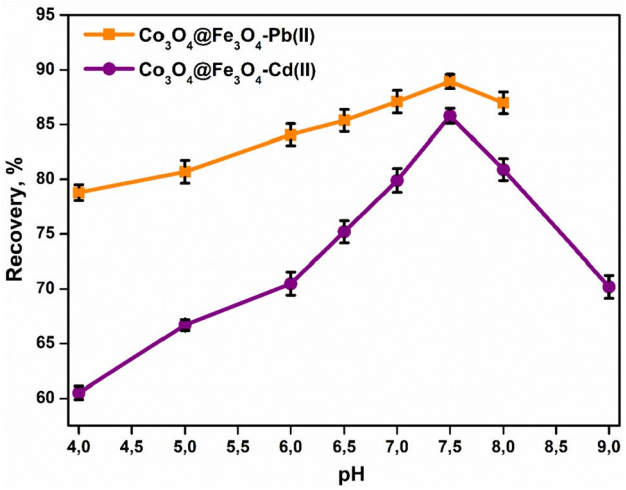

Fig. 5 Effect of pH on Pb^{2+} and Cd^{2+} recovery (amount of Co_3O_4@Fe_3O_4: 50 mg; eluent volume: 25 mL; sonication period: 10 min, for both Pb^{2+} and Cd^{2+})

Different reports indicate that Co-based materials could exhibit ferromagnetic characteristics. The hysteresis plot of the Co_3O_4@Fe_3O_4 nanoflowers indicates that they were exposed to cation diffusion, and thus that cobalt ions spread in magnetite. Such a case might alter the superparamagnetic structure of Fe_3O_4-based nanoparticles and force Co_3O_4@Fe_3O_4 nanoflowers to exhibit ferromagnetic characteristics (Hasanoğlu Özkan et al. 2022).

Adsorption results for nanoflowers

To optimize the Co_3O_4@Fe_3O_4 nanoflowers for the recovery of Pb^{2+} and Cd^{2+} heavy metal ions, eluent type, pH, adsorbent amount, starting sample volume, extraction duration, and repeatability were studied, the results of which are shown in the following sections. While, evaluating the results of the analyses in the study, the data were evaluated by performing five repeated analyses. Calculations were made at 95% confidence level ($t = 2.78$ probability with $n-1$ degree of freedom).

pH scan

pH optimization was studied using Co_3O_4@Fe_3O_4 nanoflowers for the recovery of Pb^{2+} and Cd^{2+} heavy metal ions. To investigate this, recovery experiments were conducted at various pH ranges from 4.0 to 8.0, as shown in Fig. 5. Increased recoveries were achieved for both Pb^{2+} and Cd^{2} heavy metal ions. Figure 5 illustrates pH-related Pb^{2+} and Cd^{2+} heavy metal ion recovery rates in the presence of Co_3O_4@Fe_3O_4 nanoflowers. The highest recovery was achieved at pH 7.5 at 88.95% and 85.8% for Pb^{2+} and Cd^{2+}, respectively.

Eluent type scan

Eluent type was investigated to determine the optimum conditions for Pb^{2+} and Cd^{2+} recovery in the presence of Co_3O_4@Fe_3O_4 nanoflowers. Here, 0.1, 1, 2, 3 M HNO_3 and 1 M HCl were used as eluents. The recovery values obtained by analysing the eluent type and concentration with five repetitions are shown in Fig. 6. The highest recovery was achieved using 1 M HNO_3 at 88.1% for both Pb^{2+} and Cd^{2+} heavy metal ions.

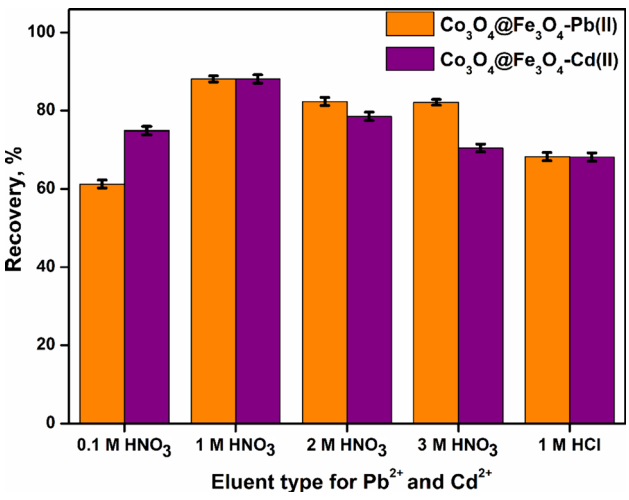

Fig. 6 Effect of eluent type for Pb^{2+} and Cd^{2+} recovery (solution pH: 7.5; amount of Co_3O_4@Fe_3O_4: 50 mg; eluent volume: 25 mL; sonication period: 10 min, for both Pb^{2+} and Cd^{2+})

Adsorbent amount scan

Optimization of the amount of adsorbent was studied for 50, 100, 150, and 200 mg Co_3O_4@Fe_3O_4 nanoflowers for Pb^{2+} and Cd^{2+} heavy metal recovery, the results of which are shown in Fig. 7. The highest recovery rate achieved for Pb^{2+} was 92.2% for 100 mg adsorbent. The highest recovery achieved for Cd^{2+} was 88.6% for 200 mg adsorbent. An increasing recovery rate was achieved with increasing amount of adsorbent for Cd^{2+} heavy metal ions. The recovery rate for Pb^{2+} was found to be Gaussian in nature, where the highest recovery was achieved for 100 mg adsorbent, after which an increasing amount of adsorbent resulted in a decreased recovery rate.

Eluent volume scan

Optimization of the volume of solvent was studied for 5 mL, 10 mL, 20 mL, and 30 mL for Pb^{2+}, and 2.5 mL, 5 mL, 10 mL, 20 mL, and 30 mL for Cd^{2+} heavy metal ion recovery in the presence of Co_3O_4@Fe_3O_4 nanoflowers. The eluent type-related recovery characteristics of the Co_3O_4@Fe_3O_4 nanoflowers are shown in Fig. 8. The highest Cd^{2+} recovery was achieved with a 5 mL solvent volume at 96.9%. Decreased Cd^{2+} recovery was observed for increasing solvent volumes. The highest recovery for Pb^{2+} was achieved at a solvent volume of 20 mL at 97.3%. Different eluent volumes give different recovery rates for different heavy metals; therefore, 20 mL and 5 mL eluent volumes showed the maximum recoveries of Pb^{2+} and Cd^{2+} ions, respectively.

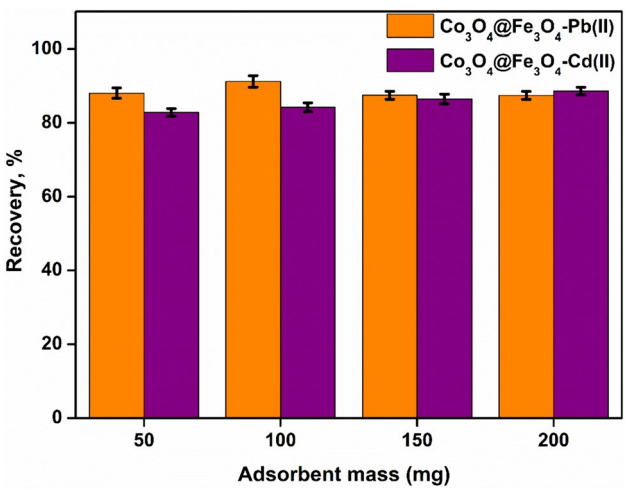

Fig. 7 Effect of amount of adsorbent on the recovery of Pb^{2+} and Cd^{2+} (solution pH: 7.5; eluent volume: 25 mL; sonication period: 10 min)

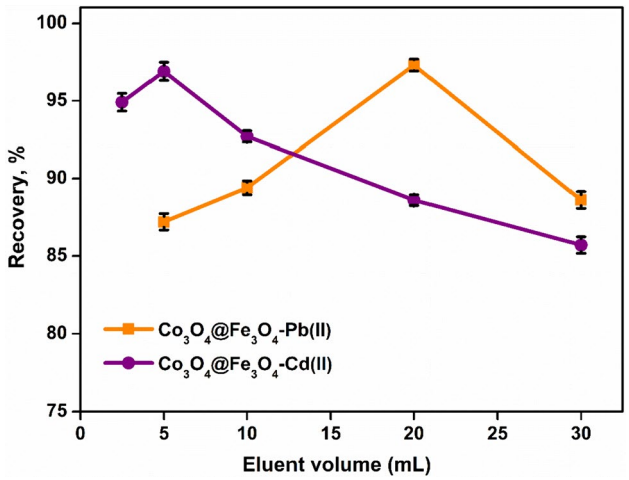

Fig. 8 Effect of sample volume on the recovery of Pb^{2+} and Cd^{2+} (solution pH: 7.5; sonication period: 10 min; amount of Co_3O_4@Fe_3O_4: 100 mg and 200 mg for Pb^{2+} and Cd^{2+}, respectively)

Extraction duration

The effect of extraction duration on Pb^{2+} and Cd^{2+} ion recovery was studied in the presence of Co_3O_4@Fe_3O_4 nanoflowers. Extraction durations were studied for 5, 10, 20, 30, and 60 min, and the recovery rates shown in Fig. 9. The highest recovery was achieved for 30 min extraction for both Pb^{2+} and Cd^{2+} heavy metal ions. Recovery rates for Pb^{2+} and Cd^{2+} heavy metal ions were determined to be 99.6% and 99.9%, respectively. Optimum recovery conditions were determined and are shown in Table 2.

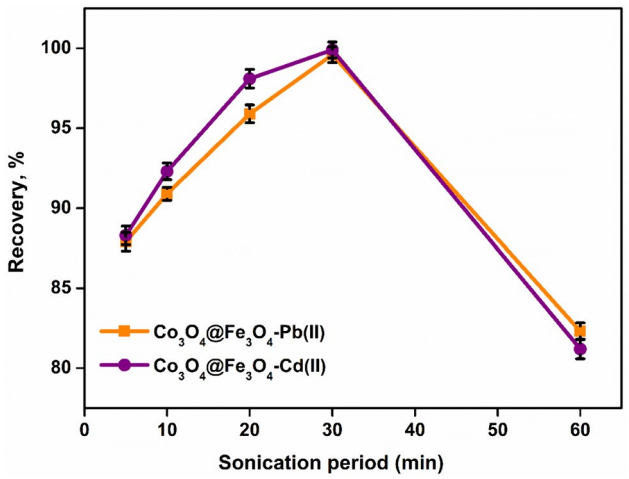

Fig. 9 Effect of extraction duration on the recoveries of Pb^{2+} and Cd^{2+} (solution pH: 7.5; amount of Co_3O_4@Fe_3O_4: 100 mg and 200 mg; eluent volume: 20 mL and 5 mL; for Pb^{2+} and Cd^{2+}, respectively)

Table 2 Optimum conditions for the Co_3O_4@Fe_3O_4 enrichment process (95% confidence level)

Heavy metal ions	Eluent type	pH	Adsorbent amount (mg)	Eluent volume (mL)	Sonication period (min)
Pb^{2+}	1 M HNO_3	7.5	100	20	30
Cd^{2+}	1 M HNO_3	7.5	200	5	30

Table 3 Parameters relating to the validation of the metal ions ($n=12$, 95% confidence level)

	Pb^{2+}	Cd^{2+}
Linear regression ($y=ax+b$)	0.0737x − 0.0015	0.03x + 0.0039
RSD%	0.2–2.4	0.4–4.8
LOD, mg/L	0.002	0.0018
Correlation coefficients (R^2)	0.9992	0.9995
LOQ, mg/L	0.007	0.006

Table 4 Effect of foreign ions on Pb^{2+} and Cd^{2+} heavy metal ion recovery (Sample volume: 25 mL, amount of Pb^{2+} and Cd^{2+}: 25 µL from 50 mg/L, $n=5$. 95% confidence level)

Ions	Added	Added, mg/L	Pb^{2+}	Cd^{2+}
Na^+	NaCl	250	101 ± 1	99.3 ± 0.2
K^+	KCl	100	99.9 ± 0.3	98.7 ± 0.9
Ca^{2+}	$CaSO_4.2H_2O$	100	102 ± 1	95.7 ± 0.8
Cu^{2+}	$Cu(NO_3)_2$	0.25	97.2 ± 0.3	95.4 ± 0.3
Fe^{2+}	$Fe(NO_3)_2.6H_2O$	0.5	94.8 ± 0.5	98.9 ± 0.2
Ni^{2+}	$Ni(NO_3)_2.6H_2O$	0.25	99.9 ± 0.1	98.6 ± 0.2
Zn^{2+}	$ZnSO_4.7H_2O$	2.5	99.6 ± 0.3	98.6 ± 0.1
Mn^{2+}	$Mn(NO_3)_2.4H_2O$	0.1	96.8 ± 0.1	96.9 ± 0.1

Validation parameters for linearity, limit of detection (LOD), limit of quantification (LOQ), and relative standard deviation (RSD%) for the metals are shown in Table 3.

Matrix interference is a physical interference, and can either suppress or enhance absorbance signal of analyte. For this effect of foreign ions on heavy metal removal was investigated in a solid-phase extraction study which was conducted in the presence of Co_3O_4@Fe_3O_4 nanoflowers. It could be seen that matrix ions in real samples do not have any apparent effect on the recovery rates of Pb^{2+} and Cd^{2+} heavy metal ions (see in Table 4). It was thus proposed that foreign ions do not interfere with the enrichment process.

The reusability of the Co_3O_4@Fe_3O_4 nanoflowers was also studied. For the reusability study, the solid-phase used in the extraction duration study was used. The adsorbent used in the extraction duration study was then washed several times using deionized water and reused for the optimization. For reusability tests, the nanomaterials obtained after the adsorption process were washed once with 1 M nitric acid and then washed three times with pure water. The presence of Pb^{2+} and Cd^{2+} in the nitric acid and pure water used in the washing process was analysed using FAAS. However, as a result of the analysis, it was seen that it was below the detection limit for metal ions. With regard to the repeatability of the nanomaterial, while we observed 99.6% and 99.6% recovery in the first use for Pb^{2+} and Cd^{2+}, respectively, these decreased to 98.2% and 98.9% after the fifth use, respectively. The average recoveries for Pb^{2+} and Cd^{2+} over the first five uses were found to be 99.0% and 99.5%, respectively. In addition, the results for the repeatability were determined over five repetitions. It should be noted that there was a negligible decrease in the recovery performance of the magnetic nanoparticles used for Pb^{2+} and Cd^{2+}.

Table 5 Analysis results for SRM seawater (NASS-6) ($n=3$)

	Pb^{2+}	Cd^{2+}
Certified value (µg/L)	0.006 ± 0.002	0.0311 ± 0.0019
Result (µg/L)	0.0063 ± 0.0002	0.0303 ± 0.0019
Recovery (%)	105 ± 1	97.4 ± 0.2

To test the reliability of the process, SRM (standard reference material) seawater (NASS-6) was used. The results pertaining to the reliability process are shown in Table 5.

The percent preconcentration factors (PF%) for Pb^{2+} and Cd^{2+} heavy metal recoveries were 200 and 260, respectively, which were evaluated via the following equation:

$$PF(\%) = C_{ap}/C_{sp} \times R \times 100,$$

where C_{ap} is the final concentration, and C_{sp} is the initial concentration of the analytes in the elution phase and initial phase, respectively. In order to calculate the PFs for the above for Pb^{2+} and Cd^{2+}, at least three repetitions were conducted for water samples.

In the enrichment process of Co_3O_4@Fe_3O_4 nanoflowers, the optimum conditions obtained for Pb^{2+} and Cd^{2+} heavy metal ion recovery were applied to the real samples (seawater, tap water, mineral water, and bottled water). Before the preconcentration method, 10 µL each of Pb^{2+} and Cd^{2+} standards were added to 25 mL water samples, and readings were taken via FAAS. After enrichment, the optimum conditions (solution pH: 7.5; sonication period: 30 min; amount of Co_3O_4@Fe_3O_4: 100 mg and 200 mg; eluent volume: 20 mL and 5 mL; for Pb^{2+} and Cd^{2+}, respectively) were applied, the results of which are shown in Table 6.

Different factors altering the recovery rate were investigated, where eluent type, pH, adsorbent amount, eluent volume and sonication time were considered with regard to Pb^{2+} and Cd^{2+} recovery. 99.9% Cd^{2+} and 99.6% Pb^{2+} recovery rates were achieved in the investigation. Nanoflowers

Table 6 Pb^{2+} and Cd^{2+} levels before and after enrichment in various samples (solution pH: 7.5; sonication period: 30 min; amount of Co_3O_4@Fe_3O_4: 100 mg and 200 mg; eluent volume: 20 mL and 5 mL; for Pb^{2+} and Cd^{2+}, respectively) ($n = 3$)

Sample	Before enrichment		After enrichment	
	Pb^{2+}, µg/L	Cd^{2+}, µg/L	Pb^{2+}, mg/L	Cd^{2+}, mg/L
Seawater	0.31 ± 0.02	0.94 ± 0.03	0.65 ± 0.01	2.43 ± 0.02
Bottled water	ND	ND	0.27 ± 0.02	2.42 ± 0.01
Tap water	ND	ND	0.19 ± 0.01	2.42 ± 0.01
Mineral water	ND	ND	0.19 ± 0.01	2.36 ± 0.02

ND: not detected

were used in different studies for heavy metal ion recovery. We compare our results with those of previous reports in Table 7, from which it can be seen that our results exhibit reasonable to good recovery characteristics.

Conclusion

In this work, Co_3O_4@Fe_3O_4 nanoflowers were produced via hydrothermal synthesis and their Pb^{2+} and Cd^{2+} heavy metal ion recovery potential investigated. An adsorption procedure was applied to seawater, tap water, and mineral water for Pb^{2+} and Cd^{2+} ion enrichment.

Hydrothermally synthesized Co_3O_4@Fe_3O_4 nanoflowers were characterized via XRD, SEM, EDX, and VSM. The results indicated that the Co_3O_4@Fe_3O_4 nanocomposites have flower-like structures that incorporate Co, Fe, and O atoms. Contamination-related signal was not observed. Magnetic characterization illustrated that the nanoflowers had ferromagnetic characteristics, which makes them a suitable candidates for magnetic filtration and magnetic solid-phase extraction applications.

Recovery rates for Pb^{2+} and Cd^{2+} heavy metal ions were calculated after solid-phase extraction using the concentration difference between the samples prior to and after the extraction process. In our investigations, optimum eluent type, pH, adsorbent type, amount of adsorbent, and solution volume were assessed to achieve maximum Pb^{2+} and Cd^{2+} heavy metal ion recovery. The highest recovery rates were found to be 99.6% and 99.9% for Pb^{2+} and Cd^{2+} heavy metal ions, respectively. A repeatability test was also performed up to 5 repetitions a slight recovery rate decrease was observed.

It was illustrated that Co_3O_4@Fe_3O_4 nanoflowers are reusable, and their recovery rates do not alter drastically with repeated tests for Pb^{2+} and Cd^{2+} heavy metal ion recovery. It was also seen that the extraction time of the Co_3O_4@Fe_3O_4 nanoflowers is quite short, and that adsorption rates are extremely high. It was also found that Co_3O_4@Fe_3O_4 nanoflowers provide good enrichment in real world samples such as seawater, tap water. Obtaining a very high heavy

Table 7 Comparison of recovery characteristics of nanoparticles

Nanoparticle type	Heavy metal ion	Recovery rate (%)	References
Bi_2S_3 nanoflowers	Pb^{2+}	100	Kurnaz Yetim et al. (2022)
Co_3O_4 nanoflowers	Cd^{2+}	99.2	Aybike et al. (2023)
Co_3O_4 nanoflowers	Cr^{6+}	98.3	Aybike et al. (2023)
ZnO nanoparticles	Cr^{3+}	95.2	Salem et al. (2017)
ZnO nanoparticles	Co^{2+}	78.6	Salem et al. (2017)
ZnO nanoparticles	Ni^{2+}	56.3	Salem et al. (2017)
Chelex-100 resin	Cu(II), Pb(II), Fe(III), Co(II), and Cr(III)	95	Soylak (2011)
Cu(II)-dibenzyldithiocarbamate precipitate	Pb	99	Tuzen et al. (2009)
Cu(II)-dibenzyldithiocarbamate precipitate	Cd	100	Tuzen et al. (2009)
Cu(II)-dibenzyldithiocarbamate precipitate	Cr	98	Tuzen et al. (2009)
ZnO nanoflowers	Pb (II)	99	Kataria et al. (2018)
ZnO nanoflowers	Co(II)	14.2	Kataria et al. (2018)
ZnO nanoflowers	Cd(II)	57.9	Kataria et al. (2018)
MgO nanoparticles	Cd(II)	99	Xiong et al. (2015)
MgO nanoparticles	Pb(II)	99	Xiong et al. (2015)
Graphene oxide decorated with triethylene-tetramine-modified magnetite	Cr(IV)	99.8	Islam et al. (2016)
Co_3O_4@FeO_3O_4 nanoparticles	Pb^{2+}	99.6	TW
Co_3O_4@FeO_3O_4 nanoparticles	Cd^{2+}	99.9	TW

TW this work

metal ion recovery rate illustrates that Co_3O_4@Fe_3O_4 nanoflowers have the potential to be used in real world scenarios and industrial applications.

In conclusion, our work illustrates that Co_3O_4@Fe_3O_4 nanoflowers have very high adsorption potential and can be used as an adsorbent material for heavy metal recovery applications. Having magnetic characteristics also enables nanoflowers to be used in magnetic filtration applications. It was found that Co_3O_4@Fe_3O_4 nanoflowers exhibit outstanding performance; therefore, have the potential to be used in applications involving the removal of heavy metals.

Supplementary Information The online version contains supplementary material available at https://doi.org/10.1007/s11696-024-03413-6.

Declarations

Conflict of interest The authors have no conflicts of interest to declare. All co-authors have seen and agree with the contents of the manuscript and there is no financial interest to report. We certify that the submission is original work and is not under review at any other publication.

References

Almomani F, Bhosale R, Khraisheh M, Almomani T (2020) Heavy metal ions removal from industrial wastewater using magnetic nanoparticles (MNP). Appl Surf Sci 506:144924. https://doi.org/10.1016/j.apsusc.2019.144924

Alp Kavlo H, Ince M, Ince OK, Ozcan C (2023) Green synthesis and encapsulation of superparamagnetic magnetite for Mercury (ii) removal: adsorption isotherms, adsorption kinetics, and thermodynamic studies. Anal Lett 1–17. https://doi.org/10.1080/00032719.2023.2178450

Altunay N, Tuzen M, Mogaddam MRA (2022) Ultrasonic-assisted dispersive liquid-liquid microextraction based on hydrophilic deep eutectic solvents: application to lead and cadmium monitoring in water and food samples. Food Addit Contam Part A 39(12):1963–1973. https://doi.org/10.1080/19440049.2022.2130997

Aybike BE, Koç MM, Yetim NK, Özcan C (2023) Sonochemical removal of highly toxic aqueous Cd^{2+} and Cr^{6+} ions using Dandelion-like Co_3O_4 nanoflowers. Open J Nano 8(1):36–49. https://doi.org/10.56171/ojn.1192105

Cheng S (2003) Effects of heavy metals on plants and resistance mechanisms. Environ Sci Pollut Res 10(4):256–264. https://doi.org/10.1065/espr2002.11.141.2/metrics

Dağci İ, Buse F, Baysak K, Ozcan C (2021) Determination of titanium in zinc ash by FAAS after digested using ultrasound-assisted extraction. Kırklareli Univ J Eng Sci 7(1):147–154. https://doi.org/10.34186/klujes.941163

Dave PN, Chopda LV (2014) Application of iron oxide nanomaterials for the removal of heavy metals. J Nanotechnol 14:398569. https://doi.org/10.1155/2014/398569

Elliott HA, Liberati MR, Huang CP (1986) Competitive adsorption of heavy metals by soils. J Environ Qual 15(3):214–219. https://doi.org/10.2134/jeq1986.00472425001500030002x

Gacía D, Arceo E, García JDD, Arceo E (2018) Renal damage associated with heavy metals: review work. Revista Colombiana De Nefrología 5(1):45–53. https://doi.org/10.22265/acnef.5.2.254

Goudarzi N (2007) Determination of trace amounts of copper in river and sea water samples by Flame Atomic Absorption Spectrometry (FAAS) after cloud-point preconcentration. J Braz Chem Soc 18(7):1348–1352. https://doi.org/10.1590/S0103-50532007000700009

Goudarzi N (2009) Solvent microextraction−Flame Atomic Absorption Spectrometry (SME−FAAS) for determination of ultratrace amounts of cadmium in meat and fish samples. J Agric Food Chem 57(3):1099–1104. https://doi.org/10.1021/jf8027057

Guevara-bernal DF, Bastos-arrieta J, Palet C, Candela AM (2022) Coffee husk and lignin revalorization: modification with Ag nanoparticles for heavy metals removal and antifungal assays. Water 14(11):1796. https://doi.org/10.3390/w14111796

Guo Z, Megharaj M, Beer M, Ming H, Rahman MM, Wu W, Naidu R (2009) Heavy metal impact on bacterial biomass based on DNA analyses and uptake by wild plants in the abandoned copper mine soils. Biores Technol 100(17):3831–3836. https://doi.org/10.1016/j.biortech.2009.02.043

Gupta VK, Singh S, Agrawal A, Jamal Siddiqi N, Sharma B (2015) Phytochemicals mediated remediation of neurotoxicity induced by heavy metals. Biochem Res Int 534769:1–9. https://doi.org/10.1155/2015/534769

Habila MA, Alothman ZA, El-Toni AM, Al-Tamrah SA, Soylak M, Labis JP (2017) Carbon-coated Fe_3O_4 nanoparticles with surface amido groups for magnetic solid phase extraction of Cr(III), Co(II), Cd(II), Zn(II) and Pb(II) prior to their quantitation by ICP-MS. Microchim Acta 184(8):2645–2651. https://doi.org/10.1007/s00604-017-2283-3

Hasanoğlu Özkan E, Aslan N, Koç MM, Kurnaz Yetim N, Sarı N (2022) Fe_3O_4 nanoparticle decorated novel magnetic metal oxide microcomposites for the catalytic degradation of 4-Nitrophenol for wastewater cleaning applications. J Mater Sci: Mater Electron 33(2):1039–1053. https://doi.org/10.1007/s10854-021-07376-2

Hedayati K, Goodarzi M, Kord M (2016) Green and facile synthesis of Fe_3O_4-PbS magnetic nanocomposites applicable for the degradation of toxic organic dyes. Main Group Met Chem 39(5–6):183–194. https://doi.org/10.1515/mgmc-2016-0027

Huang S, Gu L, Zhu N, Feng K, Yuan Ha, Lou Z, Li Y, Shan A (2014) Heavy metal recovery from electroplating wastewater by synthesis of mixed-Fe_3O_4@SiO_2/metal oxide magnetite photocatalysts. Green Chem 16(5):2696–2705. https://doi.org/10.1039/c3gc42496k

Ijomone OM, Ifenatuoha CW, Aluko OM, Ijomone OK, Aschner M (2020) The aging brain: impact of heavy metal neurotoxicity. Crit Rev Toxicol 50(9):801–814. https://doi.org/10.1080/10408444.2020.1838441

Islam A, Ahmad H, Zaidi N, Kumar S (2016) A graphene oxide decorated with triethylenetetramine-modified magnetite for separation of chromium species prior to their sequential speciation and determination via FAAS. Microchim Acta 183(1):289–296. https://doi.org/10.1007/S00604-015-1641-2

Jagirani MS, Uzcan F, Soylak M (2021) A selective and sensitive procedure for magnetic solid-phase microextraction of Lead(II) on magnetic cellulose nanoparticles from environmental samples prior to its flame atomic absorption spectrometric detection. J Iran Chem Soc 18(5):1005–1013. https://doi.org/10.1007/s13738-020-02085-9

Karaçam R, Kurnaz Yetim N, Koç MM (2020) Structural and magnetic investigation of Bi_2S_3@Fe_3O_4 nanocomposites for medical applications. J Supercond Novel Magn 33(9):2715–2725. https://doi.org/10.1007/s10948-020-05518-x

Kataria N, Garg VK (2018) Optimization of Pb (II) and Cd (II) adsorption onto ZnO nanoflowers using central composite design: isotherms and kinetics modelling. J Mol Liq 271:228–239. https://doi.org/10.1016/j.molliq.2018.08.135

Kavousi F, Goodarzi M, Ghanbari D, Hedayati K (2019) Synthesis and characterization of a magnetic polymer nanocomposite for the release of metoprolol and aspirin. J Mol Struct 1183:324–330. https://doi.org/10.1016/j.molstruc.2019.02.003

Kaya G, Ozcan C, Yaman M (2010) Flame atomic absorption spectrometric Determination of Pb, Cd, and Cu in *Pinus Nigra* L. and *Eriobotrya Japonica* leaves used as biomonitors in environmental pollution. Bull Environ Contam Toxicol 84(2):191–196. https://doi.org/10.1007/s00128-009-9865-7

Khan M, Soylak M (2022) Deep eutectic solvent based liquid-liquid microextraction of mercury in water, hair and fish with spectrophotometric determination: a green protocol. Anal Lett 56(7):1161–1173. https://doi.org/10.1080/00032719.2022.2121406

Khan I, Saeed K, Khan I (2019) Nanoparticles: properties, applications and toxicities. Arab J Chem 12(7):908–931. https://doi.org/10.1016/j.arabjc.2017.05.011

Kinaree S, Chanthai S (2014) Ultra-trace determination of Pb(II) and Cd(II) in drinking water and alcoholic beverages using homogeneous liquid-liquid extraction followed by flame atomic absorption spectrometry. Chem Pap 68(3):342–351. https://doi.org/10.2478/S11696-013-0459-9

Kurnaz Yetim N, Aslan N, Koç MM (2020a) Structural and catalytic properties of Fe_3O_4 doped Bi_2S_3 novel magnetic nanocomposites: P-nitrophenol case. J Environ Chem Eng 8(5):104258. https://doi.org/10.1016/j.jece.2020.104258

Kurnaz Yetim N, Aslan N, Sarıoğlu A, Sarı N, Koç MM (2020b) Structural, electrochemical and optical properties of hydrothermally synthesized transition metal oxide (Co_3O_4, NiO, CuO) nanoflowers. J Mater Sci: Mater Electron 31(15):12238–12248. https://doi.org/10.1007/s10854-020-03769-x

Kurnaz Yetim N, Berberoğlu EA, Aslan N, Koç MM, Özcan C (2022) Sonochemical removal of Pb (II) ions from the water medium using Bi_2S_3 nanostructres. Int J Environ Anal Chem. https://doi.org/10.1080/03067319.2022.2088288

Lin Z, Chen X, Xi Z, Lin S, Sun X, Jiang X, Tian H (2018) Individual heavy metal exposure and birth outcomes in Shenqiu County along the Huai River Basin in China. Toxicol Res 7(3):444–453. https://doi.org/10.1039/c8tx00009c

Lo SI, Chen PC, Huang CC, Chang HT (2012) Gold nanoparticle-aluminum oxide adsorbent for efficient removal of mercury species from natural waters. Environ Sci Technol 46(5):2724–2730. https://doi.org/10.1021/es203678v

Mahdavi S, Jalali M, Afkhami A (2012) Heavy metals removal from aqueous solutions using TiO_2, MgO, and Al_2O_3 nanoparticles. Chem Eng Commun 200(3):448–470. https://doi.org/10.1080/00986445.2012.686939

Mishra KP (2009) Lead exposure and its impact on immune system: a review. Toxicol Vitro 23(6):969–972. https://doi.org/10.1016/j.tiv.2009.06.014

Morrow H (2010) Cadmium and cadmium alloys. Kirk-Othmer Encycl Chem Technol. https://doi.org/10.1002/0471238961.0301041303011818.a01.pub3

Ozalp O, Soylak M (2023) Ag modified ZnO nanoflowers for the dispersive micro-solid-phase extraction of Lead(II) from food and water samples prior to its detection with high-resolution continuum source flame atomic absorption spectrometry. Talanta 253:124082. https://doi.org/10.1016/j.talanta.2022.124082

Ozcan C, Yaman M (2018) Determination of M, Pb and Cu in plant and soil samples to monitor pollution extent: comparison of Kirklareli-Elazig Cities. Turkey Fresenius Environ Bull 27(3):1319–1328

Özdemir S, Mohamedsaid SA, Kılınç E, Soylak M (2019) Magnetic solid phase extractions of Co(II) and Hg(II) by using magnetized C. Micaceus from water and food samples. Food Chem 271:232–238. https://doi.org/10.1016/j.foodchem.2018.07.067

Qian H, Pretzer LA, Velazquez JC, Zhao Z, Wong MS (2013) Gold nanoparticles for cleaning contaminated water. J Chem Technol Biotechnol 88(5):735–741. https://doi.org/10.1002/jctb.4030

Rascio N, Navari-Izzo F (2011) Heavy metal hyperaccumulating plants: How and why do they do it? And what makes them so interesting? Plant Sci 180(2):169–181. https://doi.org/10.1016/j.plantsci.2010.08.016

Raskin I, Kumar PN, Dushenkov S, Salt DE (1994) Bioconcentration of heavy metals by plants. Curr Opin Biotechnol 5(3):285–290. https://doi.org/10.1016/0958-1669(94)90030-2

Razzaz A, Ghorban S, Hosayni L, Irani M, Aliabadi M (2016) Chitosan nanofibers functionalized by TiO_2 nanoparticles for the removal of heavy metal ions. J Taiwan Inst Chem Eng 58:333–343. https://doi.org/10.1016/j.jtice.2015.06.003

Rihana-Abdallah A, Li Z, Lanigan KC (2022) Using cloud point extraction for preconcentration and determination of iron, lead, and cadmium in drinking water by flame atomic absorption spectrometry. Anal Lett 55(8):1296–1305. https://doi.org/10.1080/00032719.2021.2002349

Safinejad A, Goudarzi N, Chamjangali MA, Bagherian G (2017) Effective simultaneous removal of Pb(II) and Cd(II) ions by a new magnetic zeolite prepared from stem sweep. Mater Res Express 4(11):116104. https://doi.org/10.1088/2053-1591/aa9738

Saleh TA, Mustaqeem M, Khaled M (2022) Water treatment technologies in removing heavy metal ions from wastewater: a review. Environ Nanotechnol Monit Manag 17:100617. https://doi.org/10.1016/j.enmm.2021.100617

Salem IA, Salem MA, El-Ghobashy MA (2017) The dual role of ZnO nanoparticles for efficient capture of heavy metals and acid blue 92 from water. J Mol Liq 248:527–538. https://doi.org/10.1016/j.molliq.2017.10.060

Shishehbore MR, Afkhami A, Bagheri H (2011) Salicylic acid functionalized silica-coated magnetite nanoparticles for solid phase extraction and preconcentration of some heavy metal ions from various real samples. Chem Cent J 5(1):1–10. https://doi.org/10.1186/1752-153X-5-41

Soylak M (2011) Solid phase extraction of Cu(II), Pb(II), Fe(III), Co(II), and Cr(III) on Chelex-100 column prior to their flame atomic absorption spectrometric determinations. Anal Lett 37(6):1203–1217. https://doi.org/10.1081/AL-120034064

Soylak M, Latif E, Dogan M (2007) Solid phase extraction of trace metal ions with amberlite XAD resins prior to atomic absorption spectrometric analysis. J Trace Microprobe Tech 19(3):329–344. https://doi.org/10.1081/tma-100105049

Sultana S, Jabeen F, Sultana T, Al-Ghanim KA, Al-Misned F, Mahboob S (2019) Assessment of heavy metals and its impact on DNA fragmentation in different fish species. Braz J Biol 80(4):823–828. https://doi.org/10.1590/1519-6984.221849

Taghani A, Goudarzi N, Bagherian GA, Chamjangali MA, Amin AH (2018) Application of nanoperlite as a new natural sorbent in the preconcentration of three organophosphorus pesticides by microextraction in packed syringe coupled with gas chromatography and mass spectrometry. J Sep Sci 41(10):2245–2252. https://doi.org/10.1002/jssc.201701276

Talukder ME, Pervez MN, Jianming W, Stylios GK, Hassan MM, Song H, Naddeo V, Figoli A (2022) Ag nanoparticles immobilized sulfonated polyethersulfone/polyethersulfone electrospun nanofiber membrane for the removal of heavy metals. Sci Rep 12(1):1–16. https://doi.org/10.1038/s41598-022-09802-9

Tumturk H, Sahin F, Turan E (2014) Magnetic nanoparticles coated with different shells for biorecognition: high specific binding capacity. Analyst 139(5):1093–1100. https://doi.org/10.1039/c3an01726e

Tuzen M, Soylak M (2009) Multi-element coprecipitation for separation and enrichment of heavy metal ions for their flame atomic absorption spectrometric determinations. J Hazard Mater 162(2–3):724–729. https://doi.org/10.1016/j.jhazmat.2008.05.087

Wang Z, Zhai S, Lv J, Qi H, Zheng W, Zhai B, An Q (2015) Versatile hierarchical Cu/Fe_3O_4 nanocatalysts for efficient degradation of organic dyes prepared by a facile. Controll Hydrotherm Method

RSC Adv 5(91):74575–74584. https://doi.org/10.1039/c5ra16027h

Warner CL, Chouyyok W, Mackie KE, Neiner D, Saraf LV, Droubay TC, Warner MG, Addleman RS (2012) Manganese doping of magnetic iron oxide nanoparticles: tailoring surface reactivity for a regenerable heavy metal sorbent. Langmuir 28(8):3931–3937. https://doi.org/10.1021/la2042235

Xiong C, Wang W, Tan F, Luo F, Chen J, Qiao X (2015) Investigation on the efficiency and mechanism of Cd(II) and Pb(II) removal from aqueous solutions using MgO nanoparticles. J Hazard Mater 299:664–674. https://doi.org/10.1016/j.jhazmat.2015.08.008

Xu X, Xu C, Dai J, Hu J, Li F, Zhang S (2012) Size dependence of defect-induced room temperature ferromagnetism in undoped ZnO nanoparticles. J Phys Chem C 116(15):8813–8818. https://doi.org/10.1021/jp3014749

Yetim NK (2021) Hydrothermal synthesis of Co3O4 with different morphology: investigation of magnetic and electrochemical properties. J Mol Struct 1226:129414. https://doi.org/10.1016/j.molstruc.2020.129414

Yu B, Meyyappan M (2006) Nanotechnology: role in emerging nanoelectronics. Solid-State Electron 50(4):536–544. https://doi.org/10.1016/j.sse.2006.03.028

Zarei A, Saedi S, Seidi F (2018) Synthesis and application of Fe3O4 @ SiO2 @ Carboxyl - Terminated PAMAM dendrimer nanocomposite for heavy metal removal. J Inorg Organomet Polym Mater 28(6):2835–2843. https://doi.org/10.1007/s10904-018-0948-y

Zheng X, Pang L, Wu J, Pei L, Tan L, Yang C, Song X (2012) Contents of heavy metals in arable soils and birth defect risks in Shanxi, China: a small area level geographic study. Popul Environ 33(2–3):259–268. https://doi.org/10.1007/s11111-011-0138-0

Zheng K, Zeng Z, Tian Q, Huang J, Zhong Q, Huo X (2023) Epidemiological evidence for the effect of environmental heavy metal exposure on the immune system in children. Sci Total Environ 868:161691. https://doi.org/10.1016/j.scitotenv.2023.161691

Zhou SC, Wei CL, Wu H (2008) Damage to DNA of effective microorganisms by heavy metals: impact on wastewater treatment. J Environ Sci 20(12):1514–1518. https://doi.org/10.1016/S1001-0742(08)62558-9